Impact of Thermohaline Variability on Sea Level Changes in the Southern Ocean

Marlen Kolbe, Fabien Roquet, Etienne Pauthenet, David Nerini

JGR Oceans

RESEARCH ARTICLE
10.1029/2021JC017381

Impact of Thermohaline Variability on Sea Level Changes in the Southern Ocean

Marlen Kolbe[1,2], Fabien Roquet[2], Etienne Pauthenet[3], and David Nerini[4]

[1]Faculty of Science and Engineering, University of Groningen, Groningen, The Netherlands, [2]Department of Marine Sciences, University of Gothenburg, Gothenburg, Sweden, [3]Sorbonne University, UPMC University, Paris, France, [4]CNRS/INSU, IRD, Aix-Marseille University, University de Toulon, Mediterranean Institute of Oceanology (MIO), Marseille, France

Key Points:

- Variability of vertical thermohaline modes induces regional patterns in steric height trends in the Southern Ocean
- Steric height has risen north of the Polar Front and fallen south of it due to both thermo- and halosteric changes
- The halosteric effect in the Southern Ocean is nowhere negligible and significantly reduces the rate of sea level rise around Antarctica

Correspondence to:
M. Kolbe,
m.kolbe@rug.nl

Citation:
Kolbe, M., Roquet, F., Pauthenet, E., & Nerini, D. (2021). Impact of thermohaline variability on sea level changes in the Southern Ocean. *Journal of Geophysical Research: Oceans*, *126*, e2021JC017381. https://doi.org/10.1029/2021JC017381

Received 24 MAR 2021
Accepted 11 AUG 2021

Abstract The Southern Ocean is responsible for the majority of the global oceanic heat uptake that contributes to global sea level rise. At the same time, ocean temperatures do not change at the same rate in all regions and sea level variability is also affected by changes in salinity. This study investigates 10 years of steric height variability (2008–2017) in the Southern Ocean (30°S to 70°S) by analyzing temperature and salinity variations obtained from the GLORYS-031 model provided by the European Copernicus Marine Environment Monitoring Service. The thermohaline variability is decomposed into thermohaline modes using a functional Principal Component Analysis. Thermohaline modes provide a natural basis to decompose the joint temperature-salinity vertical profiles into a sum of vertical modes weighted by their respective principal components that can be related to steric height. Interannual steric height trends are found to differ significantly between subtropical and subpolar regions, simultaneously with a shift from a thermohaline stratification dominated by the first "thermal" mode in the north to the second 'saline' mode in the South. The Polar Front appears as a natural boundary between the two regions, where steric height variations are minimized. Despite higher melt rates and atmospheric temperatures, steric height in Antarctic waters (0–2,000 m) has dropped since 2008 due to higher salt content in the surface and upper intermediate layer and partially colder waters, while subtropical waters farther north have mostly risen due to increased heat storage.

Plain Language Summary Sea level variations on longer timescales mainly arise from mass changes or the thermo- and halosteric effects of temperature and salinity on water density. Recent variability in steric height in the Southern Ocean was investigated from 2008 to 2017 by analyzing potential temperature and salinity variations obtained from a global ocean reanalysis. The work was performed using a functional approach to a standard Principal Component Analysis that was applied on vertical temperature and salinity profiles (2,000 m). The resulting thermohaline modes contain information about the general temperature and salinity structure and their variations can be attributed to steric height changes. The results have shown that Antarctic waters above 2,000 m have dropped since 2008 due to higher salt content and colder waters, while subtropical waters farther north have mostly risen due to increased heat storage. Those spatial differences in recent steric height trends also display on the total sea level rise (SLR) observed from satellite data, which shows a significantly higher rate of SLR in subtropical waters compared to higher latitudes of the Southern Ocean.

1. Introduction

There is still insufficient understanding of processes controlling sea level variability (SLV) in the Southern Ocean. Mostly due to sparse data and its dynamic complexity, the Southern Ocean remains one of the least understood oceans. What is presently known is that it takes up the vast majority (72% ± 28%) of the global atmospheric heat content (Armour et al., 2016; Frölicher et al., 2015; Shi et al., 2018) and that Southern Ocean waters above 2,000 m depth were responsible for 35%–43% of the increase in the global Ocean Heat Content (OHC) from 1970 to 2017 (Cheng et al., 2020; Meredith et al., 2019). Studies have shown that this increase in heat uptake over the last four decades does not result in a uniform distribution of increased ocean temperature. Instead, waters north of the Antarctic Circumpolar Current (ACC) and especially at the surface show significant warming, whilst south of the ACC there is very little warming so far. However,

there is currently no scientific consensus regarding the actual causes for the observed delayed warming around Antarctica (Armour et al., 2016; Goosse et al., 2004; Li et al., 2013; Sallée et al., 2013).

Armour et al. (2016) have suggested that the dominant cause for this delayed warming trend lies in the dynamics of the meridional overturning circulation (MOC). Although the vast majority of oceanic heat uptake occurs in higher latitudes of the Southern Ocean, those areas simultaneously present those with the least amount of heat stored. The authors concluded that instead of heat being stored locally, the residual mean flow (upwelling waters along the ACC flowing equatorward) transports the absorbed heat to waters farther north. Following earlier studies, Armour et al. (2016) further noted that the strengthening and poleward shift of winds contributed to the past and present cooling of Antarctic waters through enhanced advection of cool high-latitude surface waters (Oke & England, 2004). Other explanations include a meltwater-induced freshening of waters close to Antarctica preventing the cold water to mix and sink (Kirkman IV & Bitz, 2011), as well as increased sea ice cover and wind-induced sea spray shielding radiation (Hutchinson et al., 2013; Korhonen et al., 2010). The authors stressed that especially changes in wind patterns may have previously contributed to the cooling of waters south of the ACC, but are playing a minor role in present and future changes. Indeed the ozone hole over Antarctica, which has been found to be responsible for this shift in winds, is currently recovering (Banerjee et al., 2020). Along with the surface freshening and decrease in radiation, these effects have been characterized as secondary causes contributing to the delay in Antarctic warming. With the MOC being considered as the primary cause, the authors further predict that the southernmost waters will eventually store some of the excess heat which would result in higher ocean temperatures even south of the ACC (Armour et al., 2016).

Still, there is a large uncertainty in the exact amount of ocean heat changes, which is primarily a result of poor data availability in this relatively remote area of the ocean, where both temperature (T) and salinity (S) data products have so far been scarce due to undersampling (Frölicher et al., 2015; Ishii et al., 2006; Newman et al., 2019; Pauthenet et al., 2017). Recent additions of qualitative data facilitate study investigations of the recent Southern Ocean structure and its responses to the changing climate. The present study contributes to the understanding of how recent temperature and salinity changes affect steric SLV in the Southern Ocean. All analyzes are based on data obtained from the Global ocean Reanalysis Ensemble Product (GREP) provided by the Copernicus Marine Environment Monitoring Service (CMEMS) (Storto, Masina, et al., 2019). Here potential temperature (θ) and practical salinity (S) profiles are used, in addition to sea surface height (SSH) data from satellite imagery to discuss how it compares to steric height values (calculated from θ and S) in Section 4. The θ and S profiles have been approximated into B-spline functions, which allows to apply a functional approach on the spline coefficients to obtain principal components (PCs) (Pauthenet et al., 2017; Ramsay & Silverman, 2005). As steric height changes are produced by thermal expansion (raising sea levels) and haline contraction (lowering sea levels) anomalies, the present functional Principal Component Analysis (fPCA) captures both contributions at once, instead of analyzing temperature and salinity (which are often correlated) separately. The PCs, computed on the entire domain and two sub-domains, form the basis of this study together with steric height values that were computed out of the 2,000 m θ and S profiles. Both steric height and the PCs have been analyzed and related to each other over time from a global, zonal and regional view. Lastly zonal trends of steric height were compared to the total SSH observations from altimetry.

After defining patterns and trends of steric height and the first two modes of the entire Southern Ocean, the subsequent analyzes consider interannual trends of the subtropical and the Antarctic sector individually. While the first two main modes of the domain contain the main thermohaline variations over the domain, the temporal evolution of the modes of the subtropical and the Antarctic sector and their relation to steric height is investigated in more detail.

2. Data and Methods

2.1. Data Sources

The Global ocean Reanalysis Ensemble Product is based on the four reanalyzes GLORYS2V4 (Mercator Ocean), ORAS5 (ECMWF), GloSea5 (Met Office), and C-GLORS05 (CMCC). All four reanalyzes are 3D gridded descriptions of the physical state of the ocean based on the NEMO model that were processed into

an ensemble mean. GREP data has so far shown very good performance when compared to observations and has been found to be very suitable for steric height investigations (de Souza et al., 2021; Storto, Masina, et al., 2019). The extracted data for this project constitutes monthly mean averages from 2008 to 2017 and the horizontal resolution of the grid is 0.25 which has been restricted to every second zonal and meridional grid point (80×720 points/profiles). The two central variables extracted from GREP are θ and S (in addition to SSH which is only used marginally in Section 4). θ and S profiles extracted from this product are based on in-situ data mainly from Argo floats. The coverage of Argo data in the Southern Ocean is relatively sparse compared to other oceanic areas, which at this point complicates identifying causes and implications of the results. However here the data period was chosen for a relatively well-covered time interval and depth of hydrographic observations.

2.2. Computation of Thermohaline Modes

Similar to the standard Principal Component Analysis (PCA), the aim of a fPCA lies in dimensionality reduction and feature extraction. The way it differs from standard PCA is that it is not directly applied on discrete values, but instead on continuous functions fitted on raw data (Pauthenet et al., 2017; Ramsay & Silverman, 2007). More specifically, vertical profiles of θ and S were projected on a B-spline basis and the analysis was then applied directly on the B-spline coefficients.

2.2.1. B-Spline Decomposition

Here we applied the fPCA on the GREP θ and S vertical profiles. The method requires to work on vertical profiles with a fixed vertical range. For this study, θ and S data is restricted to the upper 2,000 m, where the vast majority of steric height (η) changes is thought to happen (Gaillard et al., 2016; Levitus et al., 2012; Storto, Bonaduce, et al., 2019; Sokolov & Rintoul, 2009; Sutton & Roemmich, 2011) and where GREP is assumed to be most realistic due to the availability of data from ARGO profiling floats.

The θ and S profiles were fitted with a sum of B-spline functions. This step helps to reduce the computational load and to simulate the functional depth-related behavior of oceanographic properties. B-splines are generalized functions of the Bézier curve (Weisstein, 2009) and are commonly used if the goal is to replace a large amount of data points with a smooth function. The amount of internal knots (K) define the smoothness (and thus the accuracy). Here, each θ or S profile has been decomposed into $K = 20$ B-spline functions. For each of the horizontal stations, the information could therefore be reduced from 54 depth levels for both θ and S variables (2*54 values per profile) to 2*20 eigenfunctions per θ/S profile.

2.2.2. Functional Principal Component Analysis

Before proceeding with the fPCA decomposition, temperature and salinity variables must be nondimensionalized. Here θ and S anomalies (differences from the domain-mean temperature $= \overline{\theta}(z)$ and mean salinity $= \overline{S}(z)$ profiles) were weighted by the domain-average value of the thermal expansion coefficient (α) and the haline contraction coefficient (β), respectively. Weighted θ and S variables were then normalized by the total buoyancy variance estimated as $var(b) = var(\alpha\theta - \beta S)$. In that way, temperature and salinity are scaled depending on their relative contribution to the variations of buoyancy. For the global domain, α and β values of 1.16×10^{-4} C^{-1} and 7.66×10^{-4} PSU^{-1} were used. In the subtropical and the Antarctic domain the fPCA calculation was based on the respective α and β values of both sectors ($\alpha = 1.73 \times 10^{-4}$ C^{-1} and $\beta = 7.16 \times 10^{-4}$ PSU^{-1} in the subtropical, and $\alpha = 0.58 \times 10^{-4}$ C^{-1} and $\beta = 7.80 \times 10^{-4}$ PSU^{-1} in the Antarctic domain). The fPCA method was then applied on the normalized B-spline coefficients, yielding a set of vertical modes onto which any θ and S vertical profile can be projected (for computational details, see Pauthenet et al., 2017). A given vertical profile can then be reconstructed as,

$$\theta_j(z) = \overline{\theta}(z) + \sum_{i=1}^{N} y_{i,j} \xi_i^{\theta}(z) \quad (1)$$

$$S_j(z) = \overline{S}(z) + \sum_{i=1}^{N} y_{i,j}\xi_i^S(z) \quad (2)$$

Here $\overline{\theta}$ and $\overline{S}$ represent the domain-mean reference θ and S profiles as described above, $\xi_i^{\theta}(z)$ and $\xi_i^S(z)$ are the temperature and salinity eigenfunctions (also referred to as vertical modes), and $y_{j,i}$ is the mode-i principal component for the vertical profile j that represents each grid point and month. The number N of retained modes defines the order of truncation.

For the entire domain, as well as the subtropical and Antarctic region only, the corresponding PCs were computed on the monthly climatology (1 year of monthly means) of θ and S. On each of the three domains, the first five modes already explain around 99% of the total variance. Here the fPCA provides a set of uncorrelated, time- and space-dependent PC variables that explain the behavior of the water columns with changing depth with a single value instead of being a function of multiple fixed depth points (Pauthenet et al., 2017; Ramsay & Silverman, 2007; Viviani et al., 2005). The spatiotemporal dependence of the PC coefficients (variations of the PC values over time and space) allows the determination of trends for each grid point similar to how trends in steric height can be identified. In what follows, three different trend calculations were applied on the fPCA outputs: Linear trend slopes for each grid point (Figure 1), zonal linear mean trends based on the same trend points but as latitudinal averages (Figure 4, lower panel), and lastly seasonally detrended time series instead of straight-line trends (Figure 9, presenting temporal changes of the first mode of the subtropical and Antarctic region). Each of the PC trend analyzes provide direct information on how T and S have changed in the water column at a respective location without the need to consider depth levels.

2.3. Steric Height Computation

Steric height was computed on all T/S profiles as the geostrophic streamfunction (here the difference of the horizontal velocity at 2,000 m to that the surface). Using reference values of $S = 35.16504$ g/kg and $T = 0$C, the results represent the specific volume anomaly (Barker & McDougall, 2017; Roquet et al., 2015). Here the 54 depth vertical data points of practical salinity and potential temperature values (divided by the constant value of gravitational acceleration = 9.7963) were introduced to compute the dynamic height anomaly of each grid point and month. For presentation and comparison purposes, the outputs were converted into cm and centered around zero. Python implementations of The Gibbs SeaWater (GSW) Oceanographic Toolbox are available at http://www.teos-10.org.

3. Results

3.1. Steric Height: Present Distribution and Trends

Mapping the time mean of steric height reveals a continuous north-south gradient in steric height (Figure 1) that is, primarily related to the meridional temperature gradient. In order to regionally differentiate between the varying positive and negative trends and their underlying causes, the domain was separated into sectors based on steric height ranges. The superimposed red and blue contour lines organize the study domain into three sectors: The subtropical sector (all steric height values above 40 cm), the Antarctic sector (steric height values below −40 cm) and the sub Antarctic sector (steric height values in between). Here mainly the subtropical and Antarctic sector are discussed to allow for a clear separation between northern and southern water masses of the Southern Ocean. Figure 1 (lower panel) shows that, apart from the north-south gradient of the time-mean steric height, there are significant regional differences with a general transition from positive trends in the north toward negative trends in the South. Especially in the South Atlantic Ocean, this north-south gradient is clearly visible. In the Indian Ocean such a pattern is also present, but less clear, with deviations south of Australia and near the Agulhas current south-east of Africa, where steric height has decreased over time. From 40°S poleward, the overall trend distribution is very comparable to that of the Atlantic and West Pacific sector. Only in the East Pacific domain, a dominant decrease or increase in steric height along the latitudes is not present. Instead, steric height has fallen in the higher and lower latitudes of the study domain and risen in between. In the following, these trends are investigated and explained by analyzing variations of the main thermohaline modes of the Southern Ocean.

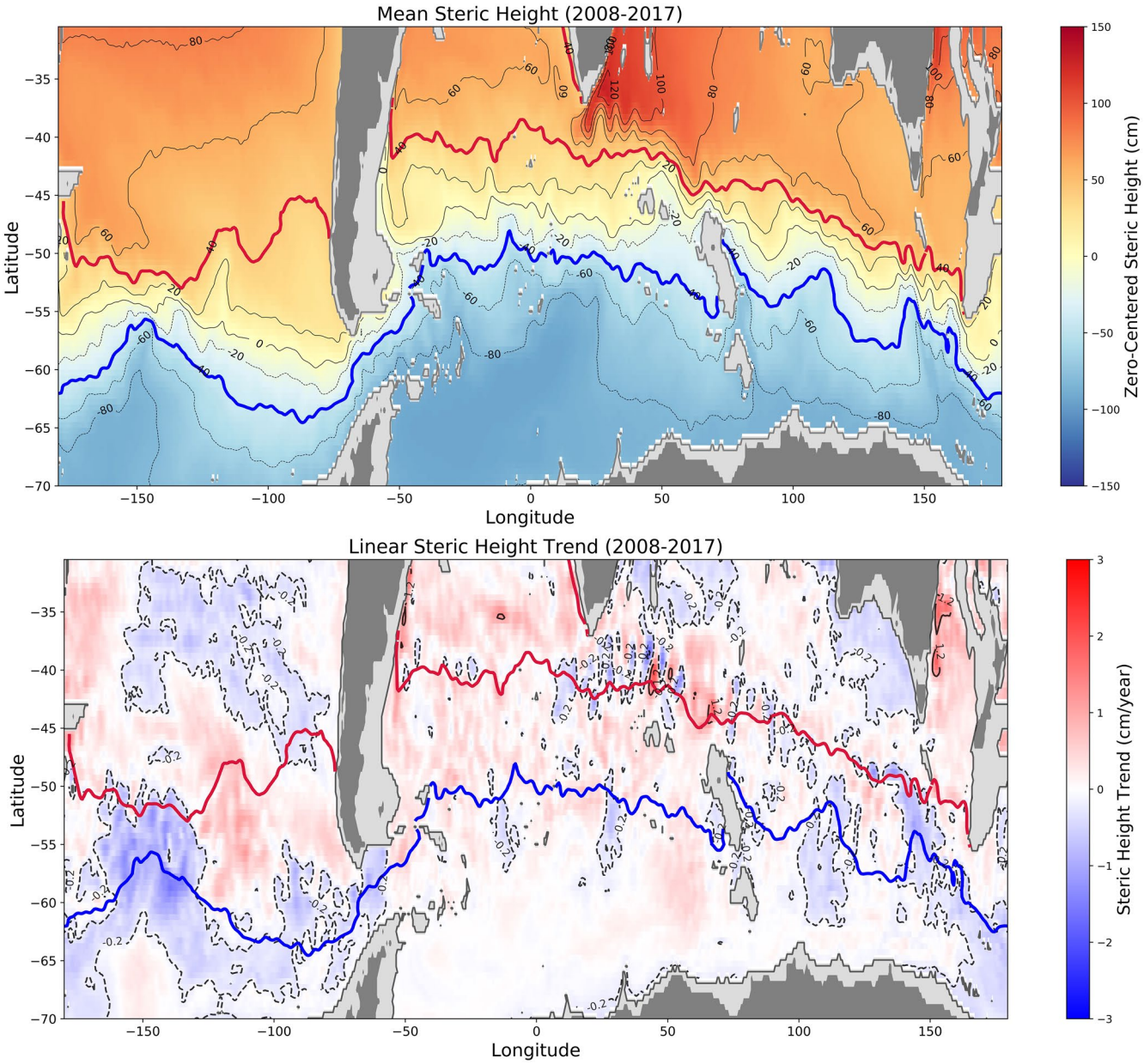

Figure 1. Upper panel: Map of the time-mean zero-centered steric height (0–2,000 m) in cm. Lower panel: Map of the linear steric height trend (0–2,000 m) in cm. Red contour lines indicate the southern limit of the subtropical sector ($\eta > 40$ cm) and blue contour lines indicate the northern limit of the Antarctic sector ($\eta < -40$ cm) chosen for this study.

3.2. Thermohaline Modes and Their Relation to Steric Height

This section evaluates the first two modes by analyzing their structure and determining the information contained with higher and lower PC values. The modes themselves do not have dimensions, but each mode conveys information about how θ and S changes with depth. For the purpose of interpreting what higher or lower PC1 and PC2 values reveal about the vertical structure of the water columns, the eigenfunctions ξ_1^{θ} and ξ_2^{S}, as calculated by the fPCA, have been added and subtracted to the mean profiles of the modes. Figure 2 illustrates those effects on the first two modes (PC1 and PC2) of the entire domain.

The resulting five thermohaline modes of the Southern Ocean combined explain 99.01% of the θ and S variance. PC1 alone already contains 84.58% of the θ and S variability. The added percentage of explained

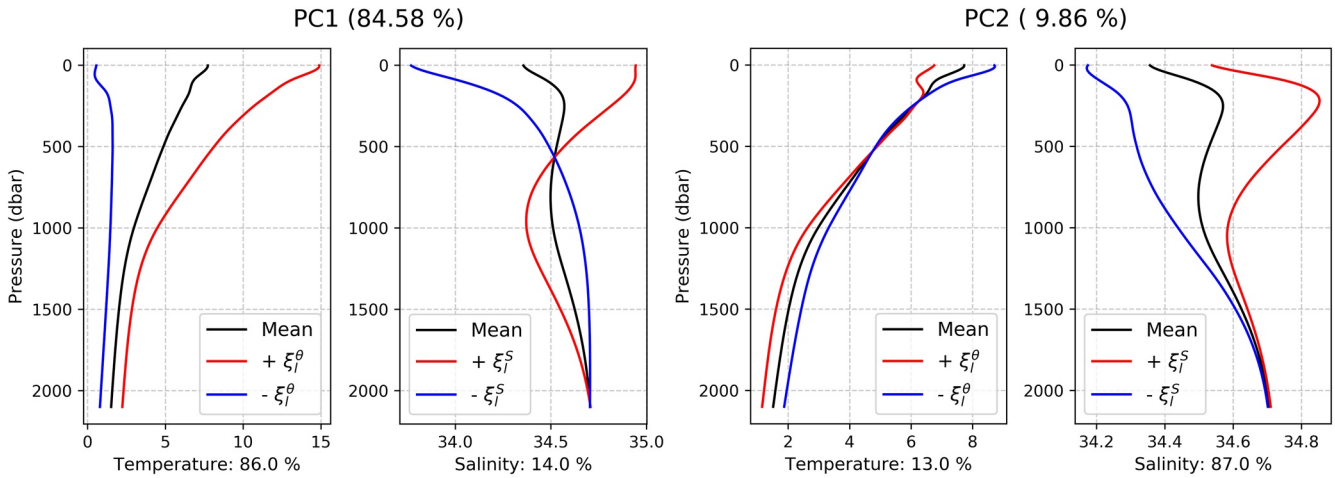

Figure 2. Global domain modes: PC1 and PC2 effect when adding (red curves) or subtracting (blue curves) the eigenfunctions of the mean profiles (black curves) computed from the climatology basis. The PC1 value has a large impact on the temperature while PC2 effects primarily the salinity.

variance for the higher modes decreases rapidly with each added mode. While the first modes (PC1 and PC2) mainly capture the prominent spatial T-S structure of the Southern Ocean (Figure 3), higher modes capture more local and complex features (Pauthenet et al., 2017) as well as seasonal variations (as the fPCA was applied on the monthly climatology). Here only the first modes are presented to put a focus on the large-scale T-S structure and its link to steric height. PC2 explains 9.86% of the averaged θ and S changes, resulting in a combined explained variance of 94.44% of PC1 and PC2 together. The split between the θ and S contribution is shown in Figure 2 just below the vertical profiles. In the case of PC1, θ plays a significantly greater role (86%) than S (14%) in altering the density of the water column, which is why it can be referred to as the thermal mode. The plotted curves in the left panel of Figure 2 reveal that a higher PC1 value represents warmer surface waters for the whole water column (0–2,000 m), particularly for the surface waters. A lower PC1 value, as represented by the red curve, implies that the temperature is more likely to remain the same with depth and is significantly colder. As for salinity, higher PC1 values indicate saltier surface waters (up to 35 PSU), while a lower value can freshen the surface to almost 33.5 PSU. Further, at around 600 m below the surface, there is an inversion, meaning that in the intermediate layer salinity decreases when PC1 increases. As temperature greatly dominates this mode, any change in PC1 is more likely to be induced by a change in temperature. Knowing that density decreases with higher temperatures, it can then be concluded that an increase in PC1 is related to an increase in steric height. Due to the dominance of θ this would apply even if there was a similar increase of salinity (which lowers steric height) over the whole water column. The lack of such a uniform increase or decrease in salinity contributes to the understanding that changes in density are mainly caused by temperature variability.

A large part of the remaining variance is explained by changes in PC2. With only 13% of the variance being explained by temperature changes, salinity dominates the second, haline mode. The right panel of Figure 2 shows that a higher value indicates more saline waters while a lower value indicates fresher waters. This is valid for the entire water column, but is more pronounced in the intermediate waters. Regarding temperature, the effect of adding and subtracting the eigenfunction is mainly impacting the surface waters, with lower temperatures related to a higher PC2 value and vice versa. Due to both the decrease in temperature and increase in salinity a higher PC2 value entails, any increase in PC2 has a negative effect on steric height.

3.3. Spatial Distribution of Modes

There is a clear large scale pattern with higher PC1 values in the subtropical part of the analyzed region and smaller PC1 values closer to the Antarctic continent (Figure 3, upper panel). The higher PC1 values in the north show the north-south temperature gradient of the surface waters that is, portrayed in the continuous north-south decline of steric sea level north of the ACC (Figure 1, lower panel). The subtropical surface waters are significantly warmer than the surface waters closer to the South Pole. Roughly, the same applies

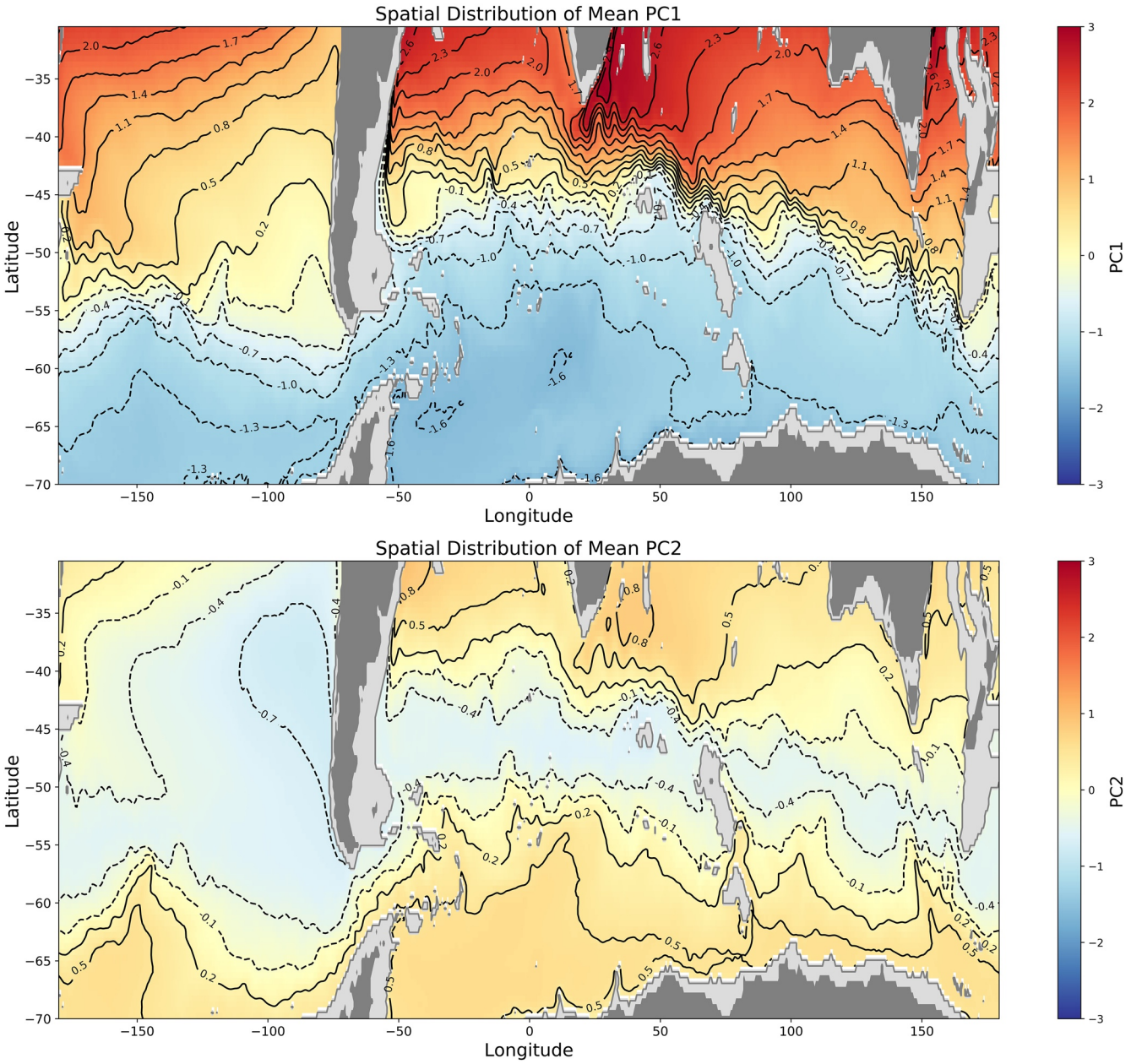

Figure 3. Spatial distribution of the temporal mean (2008–2017) of PC1 (upper panel) and PC2 (lower panel) plotted over the entire study domain.

to the salinity, with more saline surface waters in the subtropical regions and fresher waters to the South. Both of these observations are reflected in the effect of one PC unit increase of temperature and salinity respectively to the mean PC1 profile. It is evident that the θ and S gradient in the surface waters from 30°S to around 60°S dominate the overall variability of θ and S.

While PC1 alone explains a substantial part of the variance of temperature and salinity changes, it does not capture the stratification due to salinity and other more complex θ and S structures. South of 50–60°S, the PC1 value remains almost constant and thus does not capture prominent processes in the center and the southern area of the domain that could explain the steric height gradient in the Antarctic sector. The distribution of mean PC2 values over time (Figure 3, lower panel) does reveal gradients both in the subtropical part as well as closer to the pole. Instead of a continuous decrease or increase of PC2 values from north to south, there are noticeably lower PC2 values in the circumpolar region of the ACC region (wide

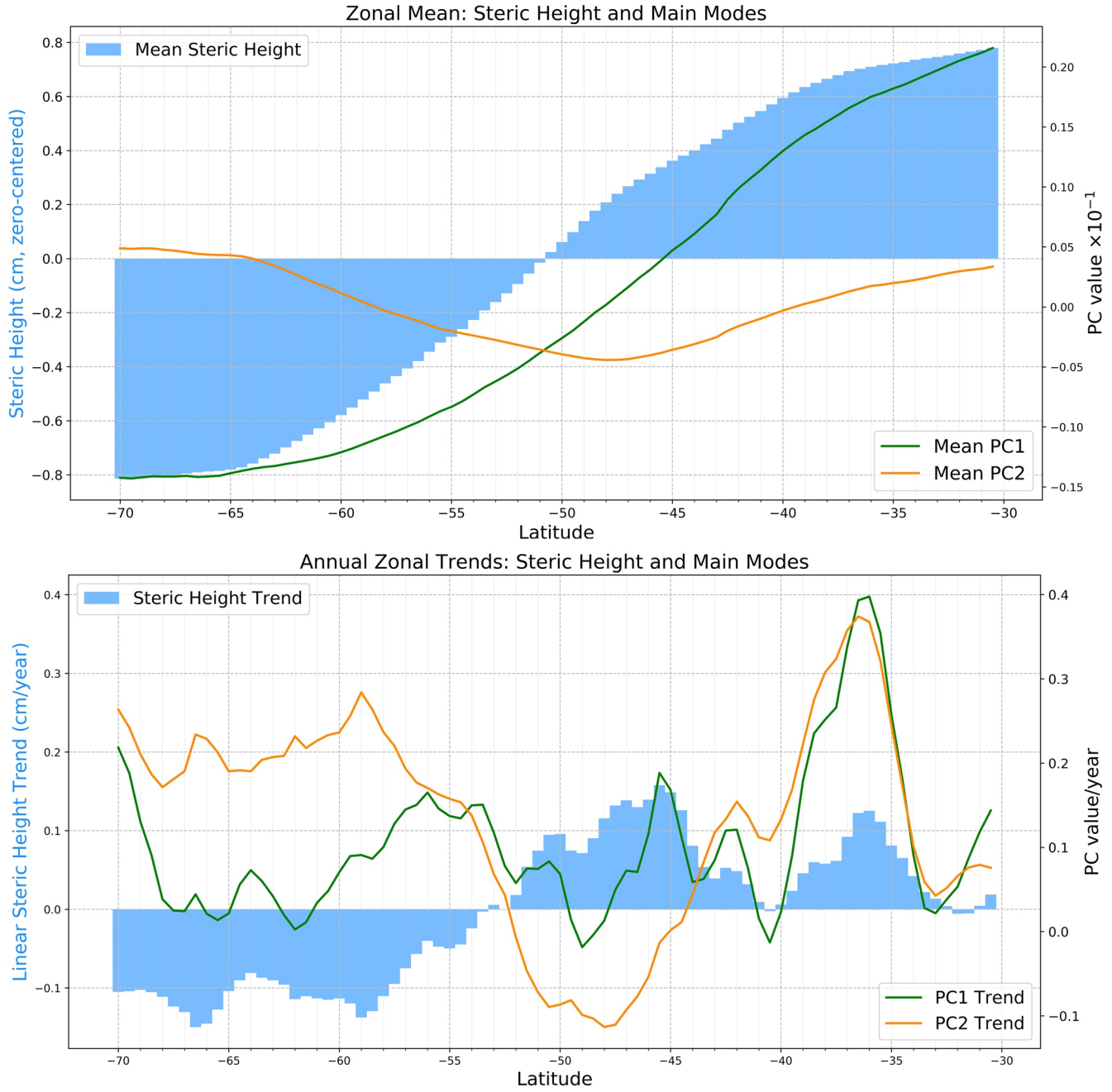

Figure 4. Upper panel: Mean steric height at every 0.5 of latitude from 30°S to 70°S. Mean values of PC1 $\times 10^{-1}$ (green) and PC2 $\times * 10^{-1}$ (orange) plotted on top. Lower panel: Linear trend slopes of steric height values for every 0.5 of latitude from 30°S to 70°S. Corresponding zonal trends of PC1 (green graph) and PC2 values (orange graph) plotted on top.

area around 50°S). With the information about what PC2 changes reveal about the vertical structure of the θ and S profiles, it can be concluded that PC2 explains the lower salinity that is, characteristic for the ACC area. It is also visible that in contrast to the longitudes of the Atlantic and Indian Ocean sectors, there is a noticeably wider area of lower PC2 values west of the South American continent. This could be attributed to the Humboldt current system transporting cold and fresh surface waters (Silva et al., 2009). The contour lines of PC2 toward the south further reveal the Polar Front (PF) and the Southern Antarctic Circumpolar Front, which could not be identified on the PC1 distribution.

This implies that the first mode is responsible for the steric height drop until roughly 50°S. As the PC1 values farther south have an almost constant value, the subsequent north-south decline in the ACC domain and farther south is a consequence of the salinity gradient captured by the second mode (Figure 3, lower panel). There is a clear gradient in PC2 from south of 50°S until 70°S from fresher to saltier waters, explaining the increase in density toward Antarctica. The increasing values of PC2 are also portraying the colder temperatures at the surface toward the Antarctic coast, as captured by the subservient effect of temperature on PC2 (Figure 2, right panel).

3.4. Regional Analysis Based on Zonal Means and Trends

Steric height south of 30°S and north of 70°S from 2007 to 2018 has risen 0.44 mm/yr on average, although this trend only follows a moderately accurate linear path. There are also large differences between regions that balance out positive and negative trends. This section analyzes zonal means and linear trend slopes, which have been computed for every 0.5 of latitude (Figure 4). It should be stressed that although a clear pattern was discovered, there are also large meridional trend gradients, that is, differences between the three main basins.

Mapping the spatial distribution of steric height (Figure 1) showed the North-South gradient that is, also clearly visible from a zonal mean perspective (Figure 4, upper panel). Steric sea levels at around 30°S are up to 1.6 m higher than those closer to the Antarctic continent. The mean values of the first two modes plotted on top provide a plausible explanation for why the steric height trends are changing between 50°S and 55°S from positive to negative, demonstrated by the zonal trend bars in the lower panel of Figure 4. The mean PC graphs cross each other in this exact zone, indicating that waters south of this zone are dominated by salinity changes, and north of it by temperature changes. It is also in this zone where the mean position of the PF is located (Kim & Orsi, 2014; Pauthenet et al., 2017, 2019), which could be identified as the southernmost front captured by the mean PC1 map (Figure 1, upper panel). The Polar Frontal Zone between the Subantarctic Front and the PF has previously been identified as the zone where the stratification of the ocean is neither dominated by temperature, nor by salinity (Pauthenet et al., 2017; Pollard et al., 2002). In the lower latitudes, it is clear that the rising temperatures have caused rising sea levels, whilst increased salinity in surface and intermediate waters seems to compensate this effect. This compensation is not only derived from the second mode, but is already contained in the first mode itself, with higher values indicating saltier surface waters. However, PC1 alone can not explain the negative trend in the south (as even south of the PF it is still mostly positive). Here the haline mode (PC2) dominates density variations and hence has caused lower sea levels as a result of increased salinity. Apart from the PF at around 53°S, there is another close to zero steric height at around 40°S at the Subtropical Front (STF), which separates the significantly warmer subtropical waters from colder waters to the South.

The general north-south trend gradient in steric height is also relevant considering the already prominent zonal decrease of mean steric height values from north to south. The respective trend gradients steepen the slope of higher steric sea levels to the north and lower levels to the South, which thereupon results in a stronger pressure gradient. Such modifications are typically reflected in an intensification of present currents. The ACC is a dominantly wind-driven current that was indeed subject to an increased transport within the last decades, related to the southern annular mode driving stronger westerly winds in recent years (Farneti et al., 2015; Fyfe et al., 2007; Langlais et al., 2015; Liau & Chao, 2017). In the Southern Hemisphere, the strengthening of winds increase the Ekman transport anomaly to the left of the wind direction due to the Coriolis force. It can be expected that the steric effect presented here contributes to the enhanced ACC transport. It is further interesting that the positive trend of PC1 is noticeably greater toward the Antarctic coast.

3.5. PC1 in the Subtropical and Antarctic Sectors

In order to rule out that such results are partly caused by correlation, the fPCA was reapplied separately on the subtropical and the Antarctic sector as defined above. This provides a more detailed picture of the main differences in the general vertical structure and allows to find out whether temperature or salinity (or both) are responsible for the regional steric height trends. The effects of the regional modes are more distinctive

of thermohaline characteristics of the two sectors. Hereafter the first mode of the subantarctic domain is called PC1-North and the first mode of the Antarctic domain is referred to as PC1-South.

One foreseeable, but important finding of the regional fPCA computation is that temperature dominates the subtropical (68%), and that salinity dominates the Antarctic density variance (78%). In the subtropical region, computing the modes results in a stronger thermocline as well as warmer mean temperature compared to PC1 with smaller deviations of maximal 2C (Figure 5, upper panel). In the upper layer, the effect with one added eigenfunction remains similar, so that higher values of the first mode are again indicative of warmer and saltier waters. Salinity changes primarily occur at the surface, where warmer waters farther north equal saltier waters. In comparison to the first mode of the entire domain (PC1), there is a low mean salinity at about 1,000 m depth, representing the Antarctic Intermediate Waters between the saltier Subantarctic Mode Water and the Upper Circumpolar Deep Water. The boundary to the subantarctic waters is too far south for PC1-North to depict the salinity inversion from before (Figure 2, right panel). The net effect on steric height is therefore less strong, since salinity compensates the decrease in density caused by higher temperatures in the whole water column. Salinity changes are now slightly dominant (54%) which is a result of a much smaller range of temperatures. The T-S percentages here are based on the same $\alpha - \beta$ ratio as calculated from the entire domain to allow a more homogeneous interpretation. Here the mean θ and S values are both significantly affecting density by offsetting each other, although the temperature gradient prevails in accounting for the steric height gradient from north to south.

In the Antarctic sector, the mean profile of PC1-South (gray temperature curve of PC1-South in Figure 5) describes the temperature effect covered by higher values of PC2 in the global domain (see Figure 2, right panel, and Figure 5, lower panel). PC1-South captures the characteristics of polar waters of having a much smaller range of temperatures, a shallow thermocline and a more distinctive mixed layer. Higher values are associated with an increase in temperature at all vertical levels (until 2,000 m). As for salinity, higher PC1-South values indicate fresher waters until 800 m below which they are slightly more salty. Temperature and salinity both significantly impact the density of the water column. The effect that this mode induces on steric height is positive, which is lightly noticeable in Figure 2, where there is a zonal steric height gradient from north to south, even if less apparent than at lower latitudes. While the global fPCA revealed the main characteristics of the Southern Ocean, these two local modes allow a more reliable conclusion on why steric height has risen or fallen over the years depending on the region.

3.6. Effect of PC1, PC1-North and PC1-South on Steric Height

Any change in steric height is a result of variations in both temperature and salinity. Therefore, steric height changes can be approximately quantified using PC1 variations for any given domain as long as the first mode captures a sufficiently large fraction of the total variance. This is the case for the three domains under consideration (global: 85%, subtropical: 74%, and Antarctic: 77%). In that case, the domain-averaged change in steric height due to temperature and salinity, respectively, is proportional to the depth-mean of the associated vertical mode times the mean PC1 change (see Table 1),

$$\Delta\eta \simeq \Delta\eta_\theta + \Delta\eta_S, \tag{3}$$

with $\Delta\eta_\theta = \alpha H\overline{\xi_1^\theta}\Delta y_1$ and $\Delta\eta_S = -\beta H\overline{\xi_1^S}\Delta y_1$ the thermosteric and halosteric domain-averaged contributions driven by variations in PC1, respectively. Here, H is the total depth of considered profiles (here $H = 2000m$), $\overline{\xi_1^\theta}$ and $\overline{\xi_1^S}$ the depth-averaged vertical modes associated with PC1, and Δy_1 the domain-averaged change of PC1. These estimates are only approximate in so far as the α and β coefficients are not constant in the ocean. However, their relative variations are sufficiently small in each sub-region to yield the correct sign and magnitude of the steric height contributions.

A unit increase of the first global mode (PC1) results in a significant warming and therefore raises steric height by 69 cm which is only slightly damped by salinity (−2 cm), resulting in a net rise of 67 cm. This first global mode is able to capture the most prominent features, but is less useful in explaining more local and complex Southern Ocean water characteristics. Here the regional modes allow for a more detailed analysis of the different structures and interannual trends. The addition of one unit to the subtropical mode (PC1-North) induces a steric height rise of 10 cm (greatly compensated by salinity), while the positive effects

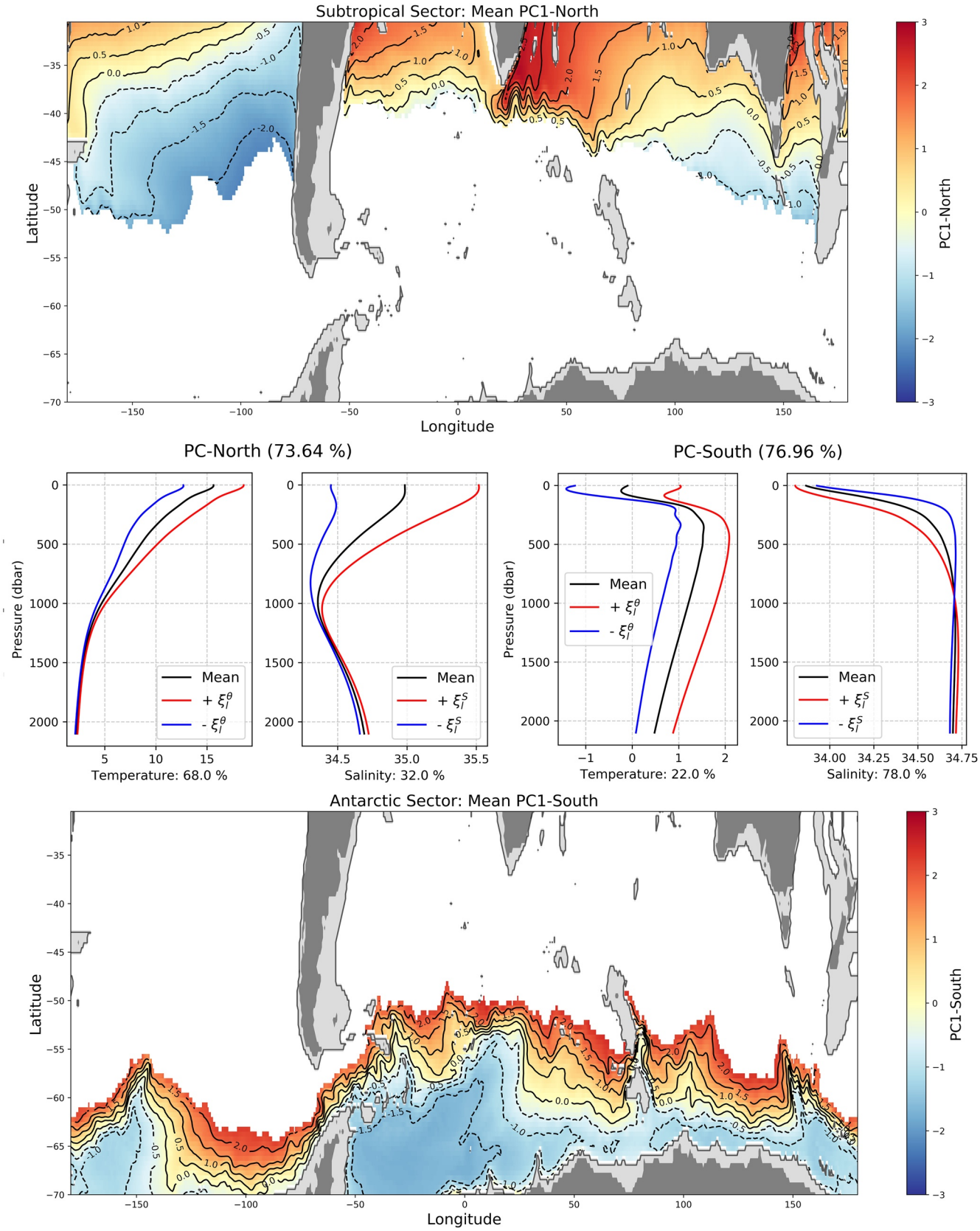
Subtropical Sector: Mean PC1-North
Latitude
Longitude
PC1-North
PC-North (73.64 %)
PC-South (76.96 %)
Pressure (dbar)
Mean
+ ξ_l^θ
- ξ_l^θ
+ ξ_l^S
- ξ_l^S
Temperature: 68.0 %
Salinity: 32.0 %
Temperature: 22.0 %
Salinity: 78.0 %
Antarctic Sector: Mean PC1-South
PC1-South

Figure 5.

Table 1
Thermal Expansion and Haline Contraction Coefficients of the Respective Domains, Along With the θ and S Effects the First Modes of Each Region Induce on Steric Height With One Added Eigenfunction

	Global Domain (PC1)	Subtropical Domain (PC1-North)	Antarctic Domain (PC1-South)
α (C^{-1})	1.16×10^{-4}	1.73×10^{-4}	0.58×10^{-4}
β (PSU^{-1})	7.66×10^{-4}	7.16×10^{-4}	7.80×10^{-4}
$\overline{\xi_1^{\theta}}$ (C)	+2.89	+0.83	+0.54
$\overline{\xi_1^{S}}$ (PSU)	+0.01	+0.13	−0.03
$\Delta\eta_{\theta}$ / Δy_1 (cm/PC)	+69	+29	+6
$\Delta\eta_{S}$ / Δy_1 (cm/PC)	−2	−19	+5
Net $\Delta\eta$ / Δy_1 (cm/PC)	+67	+10	+11

induced by temperature and salinity with an increase of one PC1-South unit increases steric height by 11 cm (Table 1).

An approximation of a spatial mean linear trend of each domain can be achieved by multiplying the linear PC trends with the respective steric height increase per PC unit ('Net $\Delta\eta/\Delta y_1$' in Table 1). For the global domain, the mean increase of $7.22 * 10^{-3}$/yr would increase the steric sea level in the Southern Ocean by 0.48 mm/yr, which is very close to the actual steric height trend of 0.44 mm/yr. Applying this approach in the two sub-domains, the predicted linear trends results in an annual rise of 0.72 mm/yr (vs. actual steric height trend: 0.87 mm/yr) in the subtropical, and a fall of −0.70 mm/yr (vs. actual steric height trend: −0.44 mm/yr) in the Antarctic domain.

Comparing the spatial trend distribution of steric height with that of PC1-North and PC1-South (Figure 6) hints to causes for the divergent regional trends. In the subtropical sector of the East Pacific, where steric height variations are mainly dependent on temperature changes, steric height has dropped due to low PC1-North values primarily indicating colder temperatures (except for waters close to the South American coastline). The Amundsen Sea has experienced decreasing temperatures as well, along with an increase in sea surface salinity (negative PC1-South trend). Those temperature and salinity trends are responsible for the differing trends visible in the East Pacific sector. As for the West Pacific sector and the Indian and Atlantic domains, the PC1-North trends dominantly suggest that the subtropical domain waters have become significantly warmer and saltier. The model θ and S data (54 levels averaged from 0 to 2,000 m) validate this information stored in the PCs. The upper panels of Figure 7 show that the positive steric height trend in the subtropical domain does mainly arise from rising temperatures, as salinity has significantly increased in most regions, lowering sea levels. Despite increased salinity and the fact that the temperature trend is not spatially consistent north of the PF and actually negative in several northern areas, the dominant positive trend of temperature has caused the subtropical increase in steric height. This finding stresses the idea that temperature has a much greater influence on SLV compared to salinity in the northern waters of the Southern Ocean.

Antarctic waters have instead become mostly colder and saltier at the surface (negative PC1-South trends, Figure 6, lower panel). Here the model data of θ and S confirm that salinity dominates the steric height evolution in very high-latitude waters. Even though temperatures have mostly risen below 65°S and partly farther north, steric height has dropped as a result of the significant increase in salinity in almost all Antarctic

Figure 5. Spatial distribution of the temporal mean (2008–2017) of the PC1-North (upper panel) and PC1-South (lower panel) domain with dashed lines indicating negative values. Profile plots in the central panel show the respective effect on PC1-North and PC1-South when adding (red curves) and subtracting (blue curves) the eigenfunctions of the respective mean profiles (black curves).

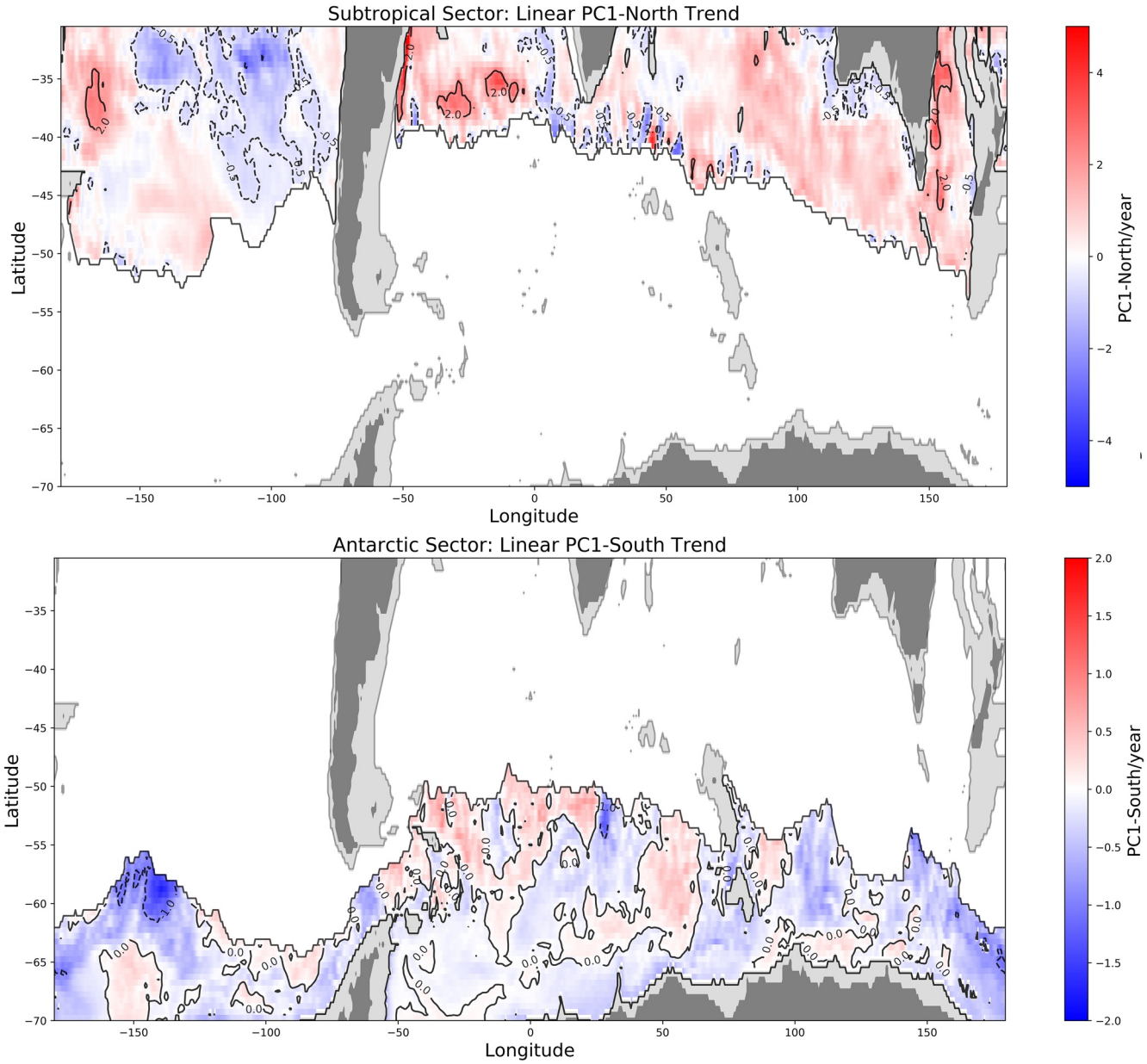

Figure 6. Map of the linear trends of the subtropical and Antarctic mode represented by the linear slope through time (from 2008 to 2017) on all grid points.

regions apart from the area near the Drake Passage (Figure 7, lower left panel). These results also explain the strikingly high PC1 values that were found closer to the Antarctic coast (Figure 4, lower panel) caused by warmer waters near the Antarctic coastline. However in the more southern sector of the ACC and most high-latitude areas in the Indian and West Pacific domain temperatures have noticeably dropped. As for the positive salinity trend, the Antarctic mode PC1-South further reveals that waters have mostly become more saline at the surface and intermediate layers instead of below 1,000 m (Figure 5, central panel on the very right). The warmer and saltier waters closer to the Antarctic coast, and colder and partly fresher waters at around 50°S to 60° support the suggestion from Armour et al. (2016) with the MOC being the main driver of the cooling trend. They also fit into the picture of a strengthening of the ACC, in that the MOC lets warm and salty water masses from the deep ocean come to the surface close to Antarctica, from where the circulation transports colder and less saline surface waters north to the ACC subduction zone.

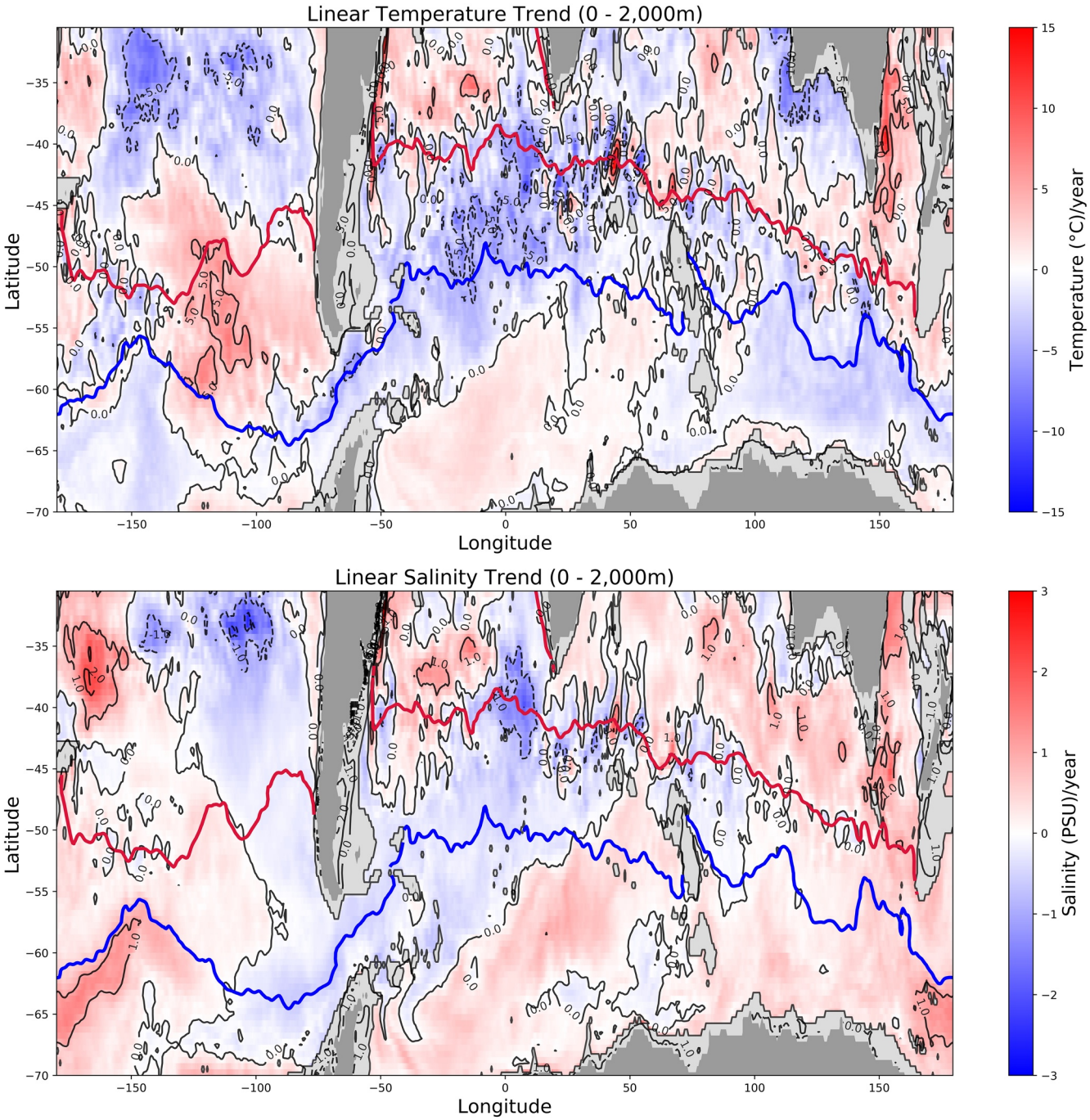

Figure 7. Maps of the linear trends of the model temperature (upper panel) and salinity (lower panel) as means of the upper 2,000 m water column, represented by the linear slope through time (from 2008 to 2017) on all grid points.

The negative PC1-South and the positive PC1-North trends display on the steric height trends (Figure 1, lower panel), raising sea levels north of the ACC and mainly lowering sea levels close to the Antarctic coast. Exceptions such as colder waters (negative PC1-North trends) south of Australia or fresher waters (positive PC1-South trends) between 50°S and 55°S in the Atlantic domain have produced opposed steric sea level trends in those regions. Although there are distinct exceptions apparent and it is thus necessary to further analyze such differences in more regional contexts, it is reasonable to distinguish between mostly rising

steric sea levels in the subtropical, and falling steric sea levels in the Antarctic domain (as demonstrated by the zonal mean trends in Figure 4).

3.7. Nonlinear Trend Variations: Subtropical and Antarctic Sector

As shown in Figure 4, PC1 and PC2 trends have indicated rising temperatures and increased salinity at almost all latitudinal ranges and vertical ranges of the water column, while steric height has risen in the subtropical and fallen in the Antarctic sector. Figure 8 shows the nonseasonal time series of steric height and the predicted nonseasonal time series of steric height based on PC1-North and PC1-South respectively, for which all PC1-North and PC1-South values have been detrended and multiplied by their regression coefficient (9.24 for PC1-North and 12.04 for PC1-South). The seasonality has been removed by applying a 12-months-centered moving average to separate the trend from the seasonality of an additive model (with the *seasonal_decompose()* function from Pythons "Statsmodels" library: http://www.statsmodels.org/stable/).

In the Antarctic sector, the predicted data follows the actual steric height course reasonably well, while in the subtropical domain the θ and S data is possibly less homogeneous which flattens the predicted steric height. The positive steric height trend in the subtropical sector is primarily arising from a nonconsistent increase from 2010 until 2014. From 2014, the monthly data outline a consistent decline in steric sea level until the beginning of 2017, reducing the linear trend to 0.9 mm/yr. From 2008 to 2017, this still signifies a trend of almost 1 cm per decade. In the Antarctic sector, the steric height results show falling sea levels from 2014 to 2016. Interestingly, both model simulations and observations have shown that the sea ice area (SIA) around Antarctica has decreased significantly since 2014, after a continuous increase in the past decades (Pu et al., 2020). Those two trends could be related to each other, as the former freshening of the Southern Ocean has been related to a northward sea ice transport introducing fresher waters farther north (Haumann et al., 2016). Following Haumann et al. (2020), the latest decrease in SIA could have caused an increase in salinity in addition to relatively colder subsurface waters as a result of a weakened stratification. This increase in salt content along with the decrease in subsurface temperature could have caused the present decline in steric height after 2014. On average, the negative trend of steric height in the southernmost waters of the Southern Ocean predicts an annual fall in steric height of −0.4 mm/yr.

The respective nonseasonal time series of PC1-North and PC1-South are shown in Figure 9. As both modes have a negative effect on density and a positive effect on steric sea level, their time series are essentially following a similar course to those of the estimated trends (Predicted η in Figure 8). Comparing the two regional modes with PC1 and PC2 of the entire domain reveals that in the subtropical domain subtropical waters have indeed gotten both warmer and saltier as suggested by the zonal trends of the first two modes in the global domain. In the Antarctic domain however, the negative trend in PC1-South indicates colder and saltier waters above 800 m depth, instead of warmer waters as could be presumed by the positive PC1 trends. Apart from correlation, those positive PC1 trends were likely a result of the salinity effect this mode captures, as higher PC1 values indicate saltier surface and fresher intermediate waters. This is a similar effect to that of decreasing PC1-South values, and could certainly be indicating increased upwelling of salty waters in the southernmost region. It should be noted that the results of the Antarctic domain are based on relatively poor observations (Sallée, 2018), which explains that there are only few studies, especially on high-latitude salinity trends. The positive temperature trends north of the ACC and the negative temperature trends in Antarctic waters however are in agreement with recent observation-based studies from Armour et al. (2016) and Auger et al. (2021).

With respect to the halosteric trend it should be noted that a Data Issue Notice has been reported by Argo that Sea-Bird conductivity cells used on floats have drifted salty, which may affect the last two years of the shown results. However it was found that the salinity drift is very minimal (extremes are filtered out) and only affects 10%–20% of the floats (More information on: https://argo.ucsd.edu/wp-content/uploads/sites/361/2020/07/salt_drift_summary_7Mar2018.pdf). Therefore it is unlikely that it would result in the abrupt negative steric height trends we see in Figure 8, which are already apparent in 2014. That being said, this drift may have contributed to the increased salinity to some degree.

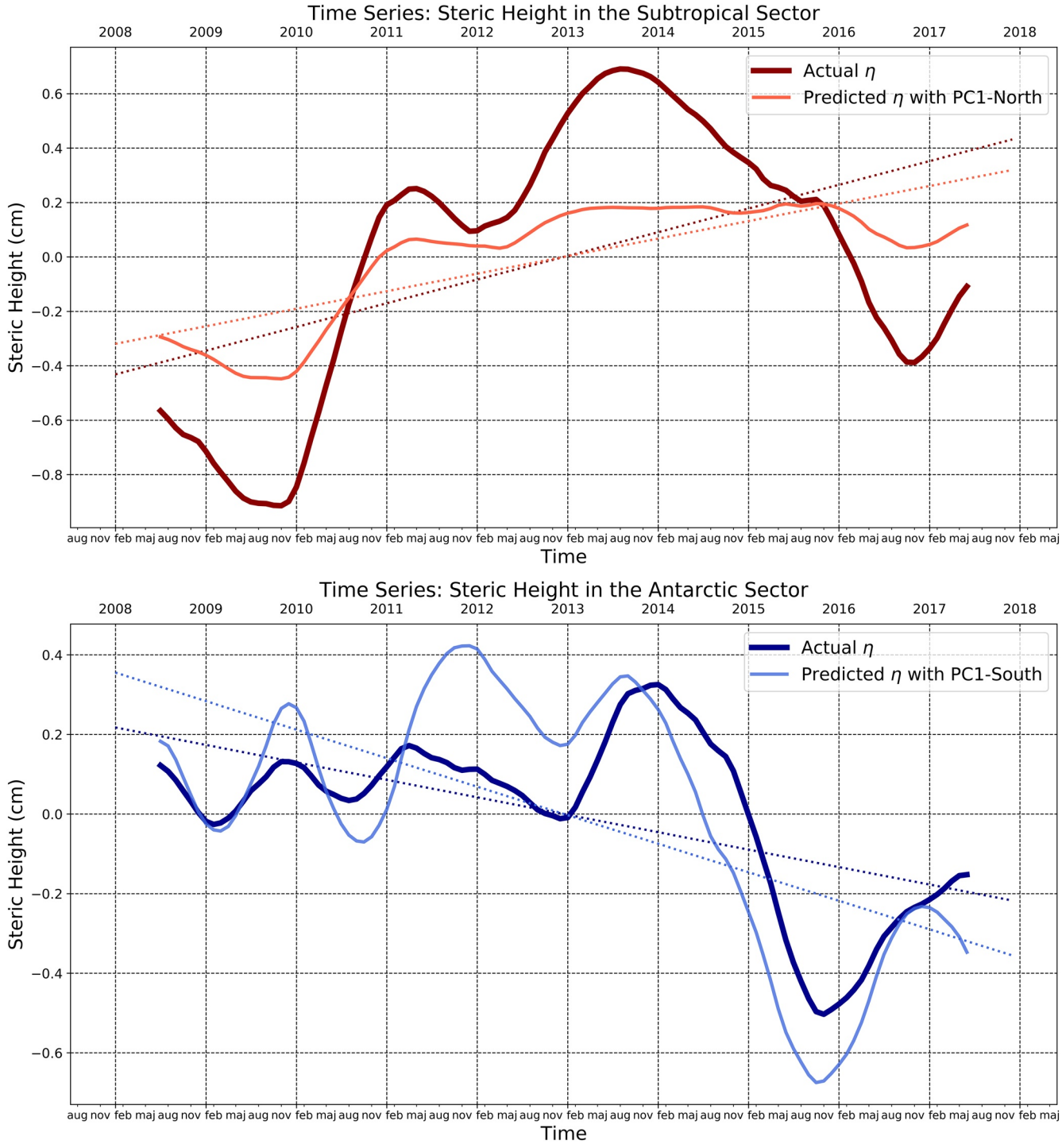

Figure 8. Nonseasonal time series of actual and predicted time series of steric height in the subtropical (upper panel) and the Antarctic (lower panel) sector from 2008 to 2017. Predictive time series of steric height are based on a linear regression model where steric height is predicted by all PC1-North (upper panel) or PC1-South (lower panel) values, and likewise detrended thereafter. Dotted lines represent the linear trends of the subtropical (Actual $\eta = 0.870$ mm/yr; Predicted $\eta = 0.644$ mm/yr) and the Antarctic (Actual $\eta = -0.438$ mm/yr; Predicted $\eta = -0.717$ mm/yr) sector.

4. Conclusions

In the present study temperature and salinity, variations were related to steric height changes in the Southern Ocean. The originality of the analysis was to first decompose the θ and S profiles into vertical thermohaline modes and to then compare the spatiotemporal evolution of the main modes with sea level varia-

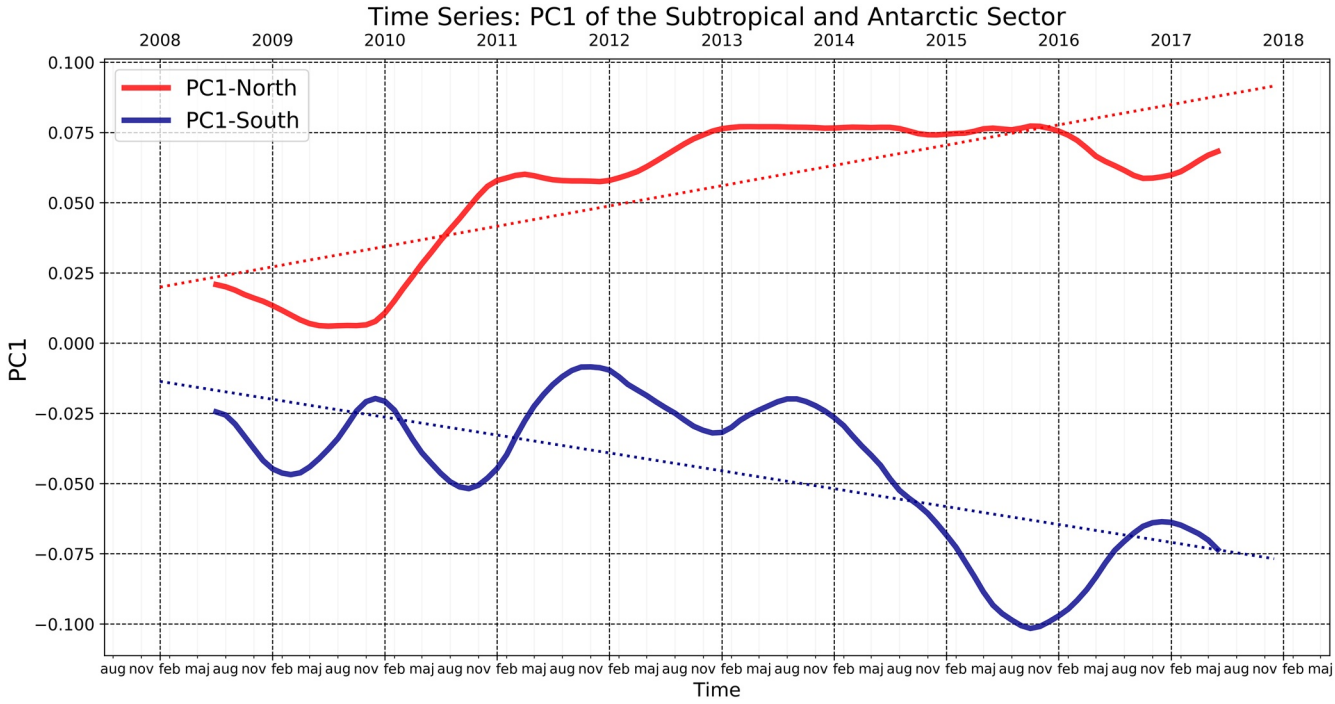

Figure 9. Nonseasonal time series of PC1 computed individually for the subtropical (red) and the Antarctic (blue) sector from 2008 to 2017. Dotted graphs show linear trends (PC1-North: $7.22 * 10^{-3}$/yr; PC1-South: $-6.37 * 10^{-3}$/yr).

tions. To generalize, the temporal analysis suggests that the salt content of the Southern Ocean's surface and intermediate layer has increased north and south of the ACC. Further the results indicate that only Antarctic waters below 800 m depth and in the Atlantic basin have experienced minor freshening (the subantarctic domain was not in the focus of this study). In the subtropical sector, especially just north of the STF (35°S to 40°S), surface and intermediate waters have become warmer and saltier. As suggested by previous studies, the cooling of Antarctic waters from the surface up to 2,000 m depth could also be identified, along with a warming trend in various regions closer to the Antarctic coast which can be associated with enhanced upwelling of deeper mater masses (Armour et al., 2016; Goosse et al., 2004; Li et al., 2013; Sallée et al., 2013). There are regional disparities at nearly all zonal ranges, but the overall trend points toward warmer and saltier subtropical, and colder and saltier (upper layer) or fresher (lower intermediate layer) waters closer to Antarctica. Higher temperatures north of the ACC portray increased oceanic heat storage from atmospheric warming, however more data over longer timescales are needed to define more certain results.

Despite the large-scale increase in salinity, the average annual trend of steric height in the Southern Ocean has increased compared to previous studies providing steric height estimations until 2015 (Ishii et al., 2006; Storto, Bonaduce, et al., 2019; von Schuckmann et al., 2010; Wang et al., 2017). In the subtropical waters of the Southern Ocean, temperature dominates the present structure of steric height, accounting for its mean distribution and its positive trend. However, despite higher temperatures in this region, the thermosteric contribution has partly been offset by a nonuniform spatial pattern of increased salinity. While in other oceans, steric height variability is largely controlled by temperature alone, salinity changes in the Southern Ocean are significantly damping the thermosteric effect of higher temperatures north of the ACC and are the dominant reason for negative steric height trends south of the ACC, where they reinforce the thermosteric effect of mostly colder waters. If these trends continue, the prominent sea level slope from north to south will further steepen which might in turn carry on altering ocean dynamics.

By encoding the leading structure of oceanographic profiles, vertical modes serve to accurately describe not only the condition and mean distribution of oceanographic properties, but can further be used to monitor present relating changes in a functional and objective way. The present study showed that the first two modes (PC1 and PC2) of the Southern Ocean can be generalized into the thermal mode in the north and

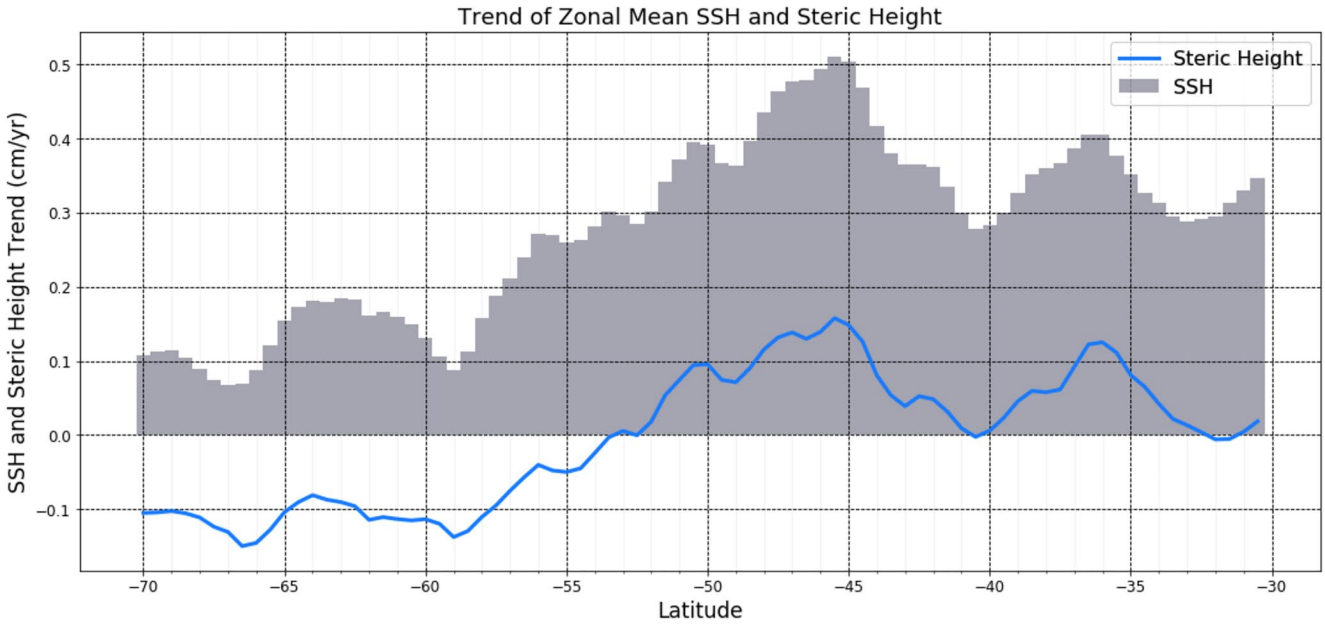

Figure 10. Linear trend slopes of steric height (blue graph) and sea surface height (gray bars) for every 0.5 of latitude from 30°S to 70°S, based on zonal means from 2008 to 2017.

the haline mode in the south (Pauthenet et al., 2017, 2019). Reapplying the fPCA on the subtropical and Antarctic sector separately confirmed the idea generated by the full-domain analysis that salinity above 2,000 m has increased in most areas. It further showed that the salinity increase in the subtropical sector occurred strongest at the surface, where salinity is already higher, while in the Antarctic sector changes are nearly evenly notable throughout the upper 1,000 m water column. Here the fPCA was applied over relatively large areas as well as monthly variations over 10 years, which puts a limitation on a clear distinction between temporal and spatial changes. However, a recent study has demonstrated a successful application of the method on very similar scales (Pauthenet et al., 2018). Based on its oceanographic application (locally/globally, at a fixed time/throughout longer time scales), the fPCA delivers a robust characterization of main variability patterns that can further be related to ocean indicators such as steric height. In part due to the significant reduction in computational load, this study provides a quantification of thermohaline variability patterns of the Southern Ocean (<2,000 m depth) and a direct relation to steric height that could not be conducted within the framework of direct T and S values at a similar cost. The time period of this study is too short to draw confident conclusions about the long-term climate trends, but serves to investigate intradecadal processes that can deviate from more linear long-term trends.

To conclusively put the steric height results into perspective with the total sea level trend, the mean linear steric height trend can be subtracted from the altimetry-based SSH data, and the zonal steric trends can be evaluated relative to zonal SSH trends (Figure 10). Total SSH has increased at all latitudes, at a rate of 0.07 cm/yr at 67°S to 0.5 cm/yr at 45°S. From 2008 to 2017, the reanalysis data suggests that the total sea level of the Southern Ocean (30°S to 70°S) has risen by 3.1 cm, of which 14% (0.44 cm) were attributed to an increase in the net thermosteric sea level. SSH in the subtropical sector showed an increase in 3.8 cm, while sea level in the Antarctic sector has only risen by 1.3 cm due to the significant compensation caused by the halosteric contribution. Despite of an average increase of Southern Ocean steric height trends compared to previous studies (Ishii et al., 2006; Storto, Bonaduce, et al., 2019; von Schuckmann et al., 2010; Wang et al., 2017), the relative steric contribution has decreased, which is likely due to accelerated melting of ice sheets and glaciers. The manometric contribution (local change in time-mean mass, (Gregory et al., 2019)) to sea level change significantly enhances the present and near future sea level rise (SLR) of Southern Ocean waters. At the same time, this study showed that steric height defines spatial patterns and can strongly influence the magnitude of recent sea level changes. The almost uniform increase in nonsteric sea levels has outweighed the steric sea level fall south of the PF and reinforced higher sea levels caused by

ocean warming in higher latitudes. In other words, the thermo- and halosteric contributions have damped the manometric SLR in Antarctic waters and significantly contributed to the SLR in subtropical waters of the Southern Ocean.

Data Availability Statement

The "GLOBAL-REANALYSIS-PHY-001-031" product was provided by the Copernicus Marine Environment Monitoring Service. Available at https://resources.marine.copernicus.eu/?option=com_csw&view=details&product_id=GLOBAL_REANALYSIS_PHY_001_031 (Accessed: April 28, 2020). The code to project vertical profiles on a B-spline basis and carry out the functional Principal Component Analysis is freely available on GitHub for R (https://github.com/EPauthenet/fda.oce) and Python (https://github.com/EPauthenet/fda_oce_python/blob/master/fda_oce_python.ipynb) environments.

Acknowledgments
Part of this work was carried out at the University of Gothenburg as a Master's thesis project under the supervision of Fabien Roquet.

References

Armour, K. C., Marshall, J., Scott, J. R., Donohoe, A., & Newsom, E. R. (2016). Southern ocean warming delayed by circumpolar upwelling and equatorward transport. *Nature Geoscience*, *9*(7), 549–554. https://doi.org/10.1038/ngeo2731

Auger, M., Morrow, R., Kestenare, E., Sallée, J.-B., & Cowley, R. (2021). Southern ocean in-situ temperature trends over 25 years emerge from interannual variability. *Nature Communications*, *12*(1), 1–9. https://doi.org/10.1038/s41467-021-22318-6

Banerjee, A., Fyfe, J. C., Polvani, L. M., Waugh, D., & Chang, K.-L. (2020). A pause in southern hemisphere circulation trends due to the Montreal protocol. *Nature*, *579*(7800), 544–548. https://doi.org/10.1038/s41586-020-2120-4

Barker, P. M., & McDougall, T. J. (2017). Stabilizing hydrographic profiles with minimal change to the water masses. *Journal of Atmospheric and Oceanic Technology*, *34*(9), 1935–1945. https://doi.org/10.1175/jtech-d-16-0111.1

Cheng, L., Abraham, J., Zhu, J., Trenberth, K. E., Fasullo, J., Boyer, T., et al. (2020). *Record-setting ocean warmth continued in 2019*. Springer.

de Souza, J. M. A. C., Couto, P., Soutelino, R., & Roughan, M. (2021). Evaluation of four global ocean reanalysis products for New Zealand waters–A guide for Regional Ocean modelling. *New Zealand Journal of Marine and Freshwater Research*, *55*(1), 132–155. https://doi.org/10.1080/00288330.2020.1713179

Farneti, R., Downes, S. M., Griffies, S. M., Marsland, S. J., Behrens, E., Bentsen, M., et al. (2015). An assessment of Antarctic circumpolar current and southern ocean meridional overturning circulation during 1958–2007 in a suite of interannual core-ii simulations. *Ocean Modelling*, *93*, 84–120. https://doi.org/10.1016/j.ocemod.2015.07.009

Frölicher, T. L., Sarmiento, J. L., Paynter, D. J., Dunne, J. P., Krastingfstort, J. P., & Winton, M. (2015). Dominance of the southern ocean in anthropogenic carbon and heat uptake in CMIP5 models. *Journal of Climate*, *28*(2), 862–886. https://doi.org/10.1175/jcli-d-14-00117.1

Fyfe, J. C., Saenko, O. A., Zickfeld, K., Eby, M., & Weaver, A. J. (2007). The role of poleward-intensifying winds on southern ocean warming. *Journal of Climate*, *20*(21), 5391–5400. https://doi.org/10.1175/2007jcli1764.1

Gaillard, F., Reynaud, T., Thierry, V., Kolodziejczyk, N., & Von Schuckmann, K. (2016). In situ–based reanalysis of the global ocean temperature and salinity with ISAS: Variability of the heat content and steric height. *Journal of Climate*, *29*(4), 1305–1323. https://doi.org/10.1175/jcli-d-15-0028.1

Goosse, H., Masson-Delmotte, V., Renssen, H., Delmotte, M., Fichefet, T., Morgan, V., et al. (2004). A late medieval warm period in the southern ocean as a delayed response to external forcing? *Geophysical Research Letters*, *31*. https://doi.org/10.1029/2003gl019140

Gregory, J. M., Griffies, S. M., Hughes, C. W., Lowe, J. A., Church, J. A., Fukimori, I., et al. (2019). Concepts and terminology for sea level: Mean, variability and change, both local and global. *Surveys in Geophysics*, *40*(6), 1251–1289. https://doi.org/10.1007/s10712-019-09525-z

Haumann, F. A., Gruber, N., & Münnich, M. (2020). Sea-ice induced southern ocean subsurface warming and surface cooling in a warming climate. *AGU Advances*, *1*(2), e2019AV000132. https://doi.org/10.1029/2019av000132

Haumann, F. A., Gruber, N., Münnich, M., Frenger, I., & Kern, S. (2016). Sea-ice transport driving southern ocean salinity and its recent trends. *Nature*, *537*(7618), 89–92. https://doi.org/10.1038/nature19101

Hutchinson, D. K., England, M. H., Santoso, A., & Hogg, A. M. (2013). Interhemispheric asymmetry in transient global warming: The role of Drake Passage. *Geophysical Research Letters*, *40*, 1587–1593. https://doi.org/10.1002/grl.50341

Ishii, M., Kimoto, M., Sakamoto, K., & Iwasaki, S.-I. (2006). Steric sea level changes estimated from historical ocean subsurface temperature and salinity analyses. *Journal of Oceanography*, *62*(2), 155–170. https://doi.org/10.1007/s10872-006-0041-y

Kim, Y. S., & Orsi, A. H. (2014). On the variability of Antarctic circumpolar current fronts inferred from 1992–2011 altimetry. *Journal of Physical Oceanography*, *44*(12), 3054–3071. https://doi.org/10.1175/jpo-d-13-0217.1

Kirkman, IV C. H., & Bitz, C. M. (2011). The effect of the sea ice freshwater flux on southern ocean temperatures in CCSM3: Deep-ocean warming and delayed surface warming. *Journal of Climate*, *24*(9), 2224–2237. https://doi.org/10.1175/2010jcli3625.1

Korhonen, H., Carslaw, K. S., Forster, P. M., Mikkonen, S., Gordon, N. D., & Kokkola, H. (2010). Aerosol climate feedback due to decadal increases in southern hemisphere wind speeds. *Geophysical Research Letters*, *37*. https://doi.org/10.1029/2009gl041320

Langlais, C. E., Rintoul, S. R., & Zika, J. D. (2015). Sensitivity of Antarctic circumpolar current transport and eddy activity to wind patterns in the southern ocean. *Journal of Physical Oceanography*, *45*(4), 1051–1067. https://doi.org/10.1175/jpo-d-14-0053.1

Levitus, S., Antonov, J. I., Boyer, T. P., Baranova, O. K., Garcia, H. E., Locarnini, R. A., et al. (2012). World Ocean heat content and thermosteric sea level change (0–2000 m), 1955–2010. *Geophysical Research Letters*, *39*. https://doi.org/10.1029/2012gl051106

Li, C., von Storch, J.-S., & Marotzke, J. (2013). Deep-ocean heat uptake and equilibrium climate response. *Climate Dynamics*, *40*(5–6), 1071–1086. https://doi.org/10.1007/s00382-012-1350-z

Liau, J.-R., & Chao, B. F. (2017). Variation of Antarctic circumpolar current and its intensification in relation to the southern annular mode detected in the time-variable gravity signals by grace satellite. *Earth, Planets and Space*, *69*(1), 93. https://doi.org/10.1186/s40623-017-0678-3

Meredith, M., Sommerkorn, M., Cassotta, S., Derksen, C., Ekaykin, A., Hollowed, A., et al. (2019). *Chapter 3: Polar Regions*.

Newman, L., Heil, P., Trebilco, R., Katsumata, K., Constable, A., van Wijk, E., et al. (2019). Delivering sustained, coordinated, and integrated observations of the southern ocean for global impact. *Frontiers in Marine Science*, *6*, 433. https://doi.org/10.3389/fmars.2019.00433

Oke, P. R., & England, M. H. (2004). Oceanic response to changes in the latitude of the southern hemisphere subpolar westerly winds. *Journal of Climate*, *17*(5), 1040–1054. https://doi.org/10.1175/1520-0442(2004)017<1040:ORTCIT>2.0.CO;2

Pauthenet, E., Roquet, F., Madec, G., Guinet, C., Hindell, M., Mcmahon, C. R., et al. (2018). Seasonal meandering of the polar front upstream of the kerguelen plateau. *Geophysical Research Letters*, *45*, 9774–9781. https://doi.org/10.1029/2018gl079614

Pauthenet, E., Roquet, F., Madec, G., & Nerini, D. (2017). A linear decomposition of the southern ocean thermohaline structure. *Journal of Physical Oceanography*, *47*(1), 29–47. https://doi.org/10.1175/jpo-d-16-0083.1

Pauthenet, E., Roquet, F., Madec, G., Sallée, J.-B., & Nerini, D. (2019). The thermohaline modes of the global ocean. *Journal of Physical Oceanography*, *49*(10), 2535–2552. https://doi.org/10.1175/jpo-d-19-0120.1

Pollard, R., Lucas, M., & Read, J. (2002). Physical controls on biogeochemical zonation in the southern ocean. *Deep Sea Research Part II: Topical Studies in Oceanography*, *49*(16), 3289–3305. https://doi.org/10.1016/s0967-0645(02)00084-x

Pu, Y., Liu, H., Yan, R., Yang, H., Xia, K., Li, Y., et al. (2020). Cas FGOALS-g3 model datasets for the CMIP6 scenario model intercomparison project (ScenarioMIP). *Advances in Atmospheric Sciences*, *37*(10), 1081–1092. https://doi.org/10.1007/s00376-020-2032-0

Ramsay, J. O., & Silverman, B. W. (2005). Principal components analysis for functional data. *Functional data analysis*, 147–172.

Ramsay, J. O., & Silverman, B. W. (2007). *Applied functional data analysis: Methods and case studies*. Springer.

Roquet, F., Madec, G., McDougall, T. J., & Barker, P. M. (2015). Accurate polynomial expressions for the density and specific volume of seawater using the TEOS-10 standard. *Ocean Modelling*, *90*, 29–43. https://doi.org/10.1016/j.ocemod.2015.04.002

Sallée, J.-B. (2018). Southern ocean warming. *Oceanography*, *31*(2), 52–62. https://doi.org/10.5670/oceanog.2018.215

Sallée, J.-B., Shuckburgh, E., Bruneau, N., Meijers, A. J., Bracegirdle, T. J., & Wang, Z. (2013). Assessment of southern ocean mixed-layer depths in CMIP5 models: Historical bias and forcing response. *Journal of Geophysical Research: Oceans*, *118*, 1845–1862. https://doi.org/10.1002/jgrc.20157

Shi, J.-R., Xie, S.-P., & Talley, L. D. (2018). Evolving relative importance of the Southern Ocean and north Atlantic in anthropogenic ocean heat uptake. *Journal of Climate*, *31*(18), 7459–7479. https://doi.org/10.1175/jcli-d-18-0170.1

Silva, N., Rojas, N., & Fedele, A. (2009). Water masses in the Humboldt Current system: Properties, distribution, and the nitrate deficit as a chemical water mass tracer for equatorial subsurface water off Chile. *Deep Sea Research Part II: Topical Studies in Oceanography*, *56*(16), 1004–1020. https://doi.org/10.1016/j.dsr2.2008.12.013

Sokolov, S., & Rintoul, S. R. (2009). Circumpolar structure and distribution of the Antarctic circumpolar current fronts: 2. variability and relationship to sea surface height. *Journal of Geophysical Research*, *114*. https://doi.org/10.1029/2008jc005248

Storto, A., Bonaduce, A., Feng, X., & Yang, C. (2019). Steric sea level changes from ocean reanalyses at global and regional scales. *Water*, *11*(10), 1987. https://doi.org/10.3390/w11101987

Storto, A., Masina, S., Simoncelli, S., Iovino, D., Cipollone, A., Drevillon, M., et al. (2019). The added value of the multi-system spread information for ocean heat content and steric sea level investigations in the CMEMS GREP ensemble reanalysis product. *Climate Dynamics*, *53*(1), 287–312. https://doi.org/10.1007/s00382-018-4585-5

Sutton, P., & Roemmich, D. (2011). Decadal steric and sea surface height changes in the southern hemisphere. *Geophysical Research Letters*, *38*. https://doi.org/10.1029/2011gl046802

Viviani, R., Grön, G., & Spitzer, M. (2005). Functional principal component analysis of FMRI data. *Human Brain Mapping*, *24*(2), 109–129. https://doi.org/10.1002/hbm.20074

von Schuckmann, K., Speich, S., Gaillard, F., & Le Traon, P.-Y. (2010). Large regional contributions of ocean heat content variability, freshwater content and steric height changes. In *EGU General Assembly Conference Abstracts* (p. 11888).

Wang, G., Cheng, L., Boyer, T., & Li, C. (2017). Halosteric sea level changes during the Argo era. *Water*, *9*(7), 484. https://doi.org/10.3390/w9070484

Weisstein, E. W. (2009). *MathWorld—A Wolfram Web Resource. Bézier curve*.